Publ. Astron. Soc. Japan (2019) 71 (2), 38 (1–12)
doi: 10.1093/pasj/psy154
Advance Access Publication Date: 2019 February 6

Radiative shocks in disk accretion

Jun Fukue*

Astronomical Institute, Osaka Kyoiku University, Asahigaoka, Kashiwara, Osaka 582-8582, Japan

*E-mail: fukue@cc.osaka-kyoiku.ac.jp

Received 2018 August 27; Accepted 2018 December 26

Abstract

Radiative shock waves standing in disk accretion flows are examined under the equilibrium diffusion approximation (1T limit) in the optically thick case, taking into account the hydrostatic equilibrium in the vertical direction. In contrast to the usual one-dimensional shock, where the gas density of the post-shock region increases due to the shock compression, if the shock is sufficiently strong, the gas density in the post-shock region often decreases due to the vertical expansion behind the shock front. However, the surface density behaves like the gas density in the usual shocks, and increases up to 7 in the radiation pressure dominated shock. Hence, the vertical optical depth in the post-shock region rises, in spite of the reduction of the gas density. In addition, similar to the usual radiative shock, there appears a radiative precursor in the pre-shock region before the shock front, due to the radiative diffusion effect. We derive the overall jump conditions for the radiative shock in disk accretion flows, and solve the structure of the radiative precursor for both the gas and radiation pressure dominated cases. The solutions are quite fundamental in disk-accretion shock problems, and should be developed in various aspects.

Key words: accretion, accretion disks — protoplanetary disks — radiation: dynamics — shock waves — stars: black holes

1 Introduction

In the universe, there are various phenomena associated with shock waves, such as supernova explosions, standing shocks in winds and accretion flows, accretion shocks in the star-forming cores, bow shocks ahead of astrophysical jets, and various other outburst phenomena. Besides astrophysical phenomena, shock waves are associated with various natural phenomena, such as volcano explosions and thunderbolts, or with various artificial origins, such as supersonic planes, blasting, and nuclear bombs, or with laboratory experiments. If the shock is sufficiently strong, then the radiation energy flux and/or pressure play an essential role in the shock flows—*radiative shocks*. The radiative influence on shock waves has been investigated in many research fields, and since Zel'dovich (1957) and Raizer (1957), there have been many publications concerning radiative shocks (e.g., Zel'dovich & Raizer 1966, 2002; Weaver 1976; Mihalas & Mihalas 1984; Lacey 1988; Bouquet et al. 2000; Drake 2005, 2007; Lowrie et al. 1999; Lowrie & Rauenzahn 2007; Lowrie & Edwards 2008; Tolstov et al. 2015; Ferguson et al. 2017).

In radiative shocks, radiation emitted from the shock front generally affects both sides of the front. The radiative diffusion in the optically thick regime, or the direct radiation in the optically thin regime, transports radiation energy into both the upstream medium in the pre-shock region before the shock front and the downstream medium in the post-shock region after the front. In the pre-shock region ahead of the shock front, radiation emitted from the shock front heats up and/or ionizes the upstream medium to

make the *radiative precursor*, whereas far from the shock there remains the undisturbed upstream medium. Even if the upstream medium is optically thick, the radiative precursor can be formed by radiative diffusion. In the post-shock region after the shock front, the downstream medium is also heated up by the shock transition, and emits radiation (*radiative zone*). Even if the downstream medium is optically thick, the relaxation zone may appear, as a region, where radiation and matter equilibrate.

The important quantity for the radiative shock behavior is the optical depth of the upstream and downstream regions (cf. Drake 2005). If both sides of the shock front are optically thick, the medium may be in local thermodynamic equilibrium (LTE) everywhere. If, further, both sides are sufficiently thick, one may often use the *equilibrium diffusion approximation*, where radiation and matter equilibrates with the same temperatures ($1T$ limit).

In the field of astrophysical accretion flows (Kato et al. 1998, 2008; figure 1), the standing shocks in disk accretion with low angular momentum were first investigated by Fukue (1987). He examined the transonic disk accretion onto a central black hole with a full relativistic treatment, using rigorous equations of state, and found multiple critical points as well as a transition through standing shocks.

Fukue (1987) assumed that the disk thickness does not alter before and after the shock for simplicity (figure 1a). On the other hand, Chakrabarti (1989) considered the hydrostatic balance in the vertical direction, and considered the accretion shock problems (see also Chakrabarti 1996; Lu & Yuan 1997; Das 2002; Chakrabarti & Das 2004; Suková et al. 2017 and references therein). If the hydrostatic equilibrium holds in the post-shock region, the disk usually puffs up in the vertical direction, and the gas density does not increase, but decreases after the shock transition (figure 1b).

Although there have been many studies on standing shocks in disk accretion flows, all of them have considered hydrodynamical shock waves (adiabatic or isothermal) in (viscous) accretion flows, and none have yet analytically examined the radiative shocks in disk-accretion shock problems (see Okuda et al. 2004 for numerical simulations of wind flows). If, of course, the disk thickness does not change at the shock front, the radiative shock in disk accretion is nothing but the usual one-dimensional radiative shock (figure 1c). For example, a radiative precursor region appears due to the radiative diffusion effect. Furthermore, the so-called *isothermal shock* in the gas pressure dominated case, or the so-called *continuous shock* in the radiation pressure dominated case, can be realized. In addition, the density compression ratio becomes up to a factor of 7 in radiation pressure dominated shocks,

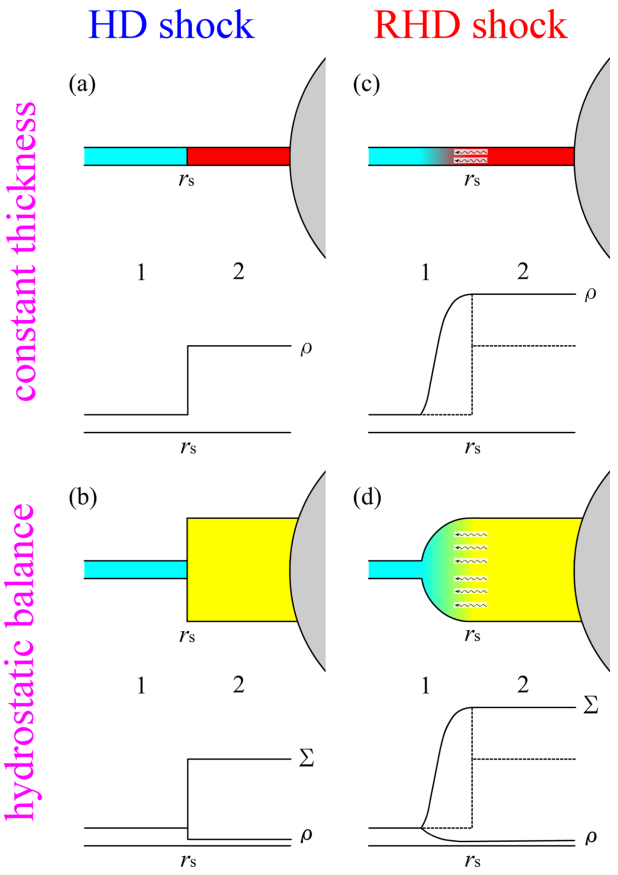

Fig. 1. Schematic pictures of disk accretion flows onto a central object with hydrodynamical (HD) nonradiative shocks or radiation-hydrodynamical (RHD) radiative shocks at r_S (upper panels in each figure), and the variations of density ρ or surface density Σ along the shock transition (lower panels in each figure). (a) HD nonradiative shocks under constant disk thickness. The gas density can increase up to a factor of 4 in the gas pressure dominated case. (b) HD nonradiative shocks under vertical hydrostatic balance. The gas density usually decreases after the shock transition, but the surface density (and optical depth) increases up to a factor of 4 if the gas pressure is dominant. (c) RHD radiative shocks under constant disk thickness; a radiative precursor appears in the pre-shock region. The density compression ratio becomes up to a factor of 7 in the radiation pressure dominated case. (d) RHD radiative shocks under vertical hydrostatic balance; a radiative precursor appears in the pre-shock region. The gas density usually decreases in the radiative precursor region, but the surface density (and optical depth) increases up to a factor of 7 if the radiation pressure is dominant. (Color online)

in contrast to 4 for gas pressure dominated shocks. If, however, we take into account the vertical hydrostatic balance after the shock front, the situation could drastically change (figure 1d).

Thus, in this paper we first examine radiative shock waves standing in disk accretion flows under the equilibrium diffusion approximation ($1T$ limit) in the optically thick case, taking into account the hydrostatic equilibrium in the vertical direction.

Since such radiative shocks in accretion flows can relate to nonrelativistic disk accretion, such as protoplanetary disks, as well as relativistic disk accretion onto a compact object, we use nonrelativistic treatments as a starting point for radiative shocks in disk-accretion shock problems.

In the next section we describe the basic equations for jump conditions and a radiative precursor, under the equilibrium diffusion approximation. We derive the overall jump conditions for the radiative shock in disk accretion flows, and solve the structure of the radiative precursor region for the gas pressure dominated case (section 3) and the radiation pressure domnated case (section 4), respectively. The final section is devoted to concluding remarks.

2 Basic equations

Except for the extremely thick case, radiation from shock fronts usually diffuses out into the pre-shock and post-shock regions, and affects the structure of shocked flows. For example, physical quantities such as temperature can continuously change in some extents, including the radiative precursor, shock front, and after-shock region.

In the present study, we consider an *equilibrium diffusion approximation* (or $1T$ limit), where the radiation temperature $T_{\rm rad}$ is equal to the gas temperature $T_{\rm gas}$ (one temperature approximation): $T_{\rm rad} = T_{\rm gas} = T$. We assume the following situations (figure 1): (i) Gas with low angular momentum accretes in the radial (r) direction onto the central object with mass M. (ii) The gas flow is optically thick, and the diffusion approximation holds. (iii) The Eddington approximation is adopted for radiation fields. (iv) Hydrostatic equilibrium is assumed in the vertical direction. (v) Change of the gravitational field or angular momentum is not considered. (vi) Radiative cooling or mass loss from the disk surface is not considered. (vii) The viscous force and magnetic fields are also dropped. (viii) The relativistic effect is also ignored. Under these assumptions, the basic equations become as follows.

2.1 Equilibrium diffusion approximation

In such a radiative shock, the radiative flux in the total energy conservation is retained, and the jump conditions for radiation and matter are derived (e.g., Lowrie & Rauenzahn 2007).

In the present study, considering the disk thickness h and hydrostatic equilibrium in the vertical direction, we can give the mass flux, momentum flux, and energy flux conservations for the gas density ρ, gas pressure p, radiation pressure P, and velocity u relative to the shock front as follows:

$$h\rho u = h_1\rho_1 u_1 = j\ (\text{constant}), \tag{1}$$

$$h(\rho u^2 + p + P) = h_1(\rho_1 u_1^2 + p_1 + P_1), \tag{2}$$

$$h\rho u\left(\frac{1}{2}u^2 + \frac{\gamma}{\gamma-1}\frac{p}{\rho} + \frac{4P}{\rho}\right) + hF = h_1\rho_1 u_1\left(\frac{1}{2}u_1^2 + \frac{\gamma}{\gamma-1}\frac{p_1}{\rho_1} + \frac{4P_1}{\rho_1}\right), \tag{3}$$

where the subscript "1" represents the quantities in the upstream region far from the shock front, and no subscript means those in other regions, including the downstream region far from the shock front (subscript "2"). Under the Eddington approximation, we have set the radiation energy density E as $E = 3P$.

The diffusive flux F is expressed in terms of the radiation pressure or temperature as a function of the coordinate x along the shock flow:

$$F = -\frac{c}{\kappa\rho}\frac{dP}{dx} = -\frac{4acT^3}{3\kappa\rho}\frac{dT}{dx}, \tag{4}$$

which is the first moment equation (diffusion form). Here, κ is opacity and assumed to be constant.

In addition, the hydrostatic equilibria in the vertical direction in the post-shock and pre-shock regions are, respectively,

$$\frac{GM}{r^3}h^2 = \frac{p+P}{\rho}, \tag{5}$$

$$\frac{GM}{r_1^3}h_1^2 = \frac{p_1+P_1}{\rho_1}, \tag{6}$$

or can be combined into the form:

$$h^2\frac{\rho}{p+P} = h_1^2\frac{\rho_1}{p_1+P_1}, \tag{7}$$

where r is the distance from the center, and we assume $r = r_1$ in the present study. Rigorously speaking, the radiative shock is not discontinuous, but has some width as a radiative precursor, and therefore $r \neq r_1$ and the gravitational field changes during the shock transition in the present accretion shock problem. As a first step, however, we ignore the change of the gravitational field (and also the angular momentum).

These equations are supplemented by the equation of state and the opacity expression.

2.2 Overall jump conditions

Far from the shock, radiation and matter equilibrate, and the diffusive flux can be ignored. Hence, for ideal gases and

isotropic radiation fields, the overall jump conditions in the present case are

$$h_2\rho_2 u_2 = h_1\rho_1 u_1 = j, \tag{8}$$

$$h_2(\rho_2 u_2^2 + p_2 + P_2) = h_1(\rho_1 u_1^2 + p_1 + P_1), \tag{9}$$

$$\frac{1}{2}u_2^2 + \frac{\gamma}{\gamma-1}\frac{p_2}{\rho_2} + \frac{4P_2}{\rho_2} = \frac{1}{2}u_1^2 + \frac{\gamma}{\gamma-1}\frac{p_1}{\rho_1} + \frac{4P_1}{\rho_1}, \tag{10}$$

$$\frac{h_2^2}{h_1^2} = \frac{\rho_1}{\rho_2}\frac{p_2+P_2}{p_1+P_1}, \tag{11}$$

where the subscripts "1" and "2" represent the quantities in the upstream and downstream regions far from the shock.

Similar to the hydrodynamical shock, by eliminating u_2 the energy and momentum conservations (Rankine–Hugoniot relations) become, respectively,

$$\frac{\gamma}{\gamma-1}\frac{p_2}{\rho_2} + \frac{4P_2}{\rho_2} - \left(\frac{\gamma}{\gamma-1}\frac{p_1}{\rho_1} + \frac{4P_1}{\rho_1}\right) + \frac{1}{2}\frac{\frac{h_2}{h_1}(p_2+P_2) - (p_1+P_1)}{\frac{h_2}{h_1}\rho_2 - \rho_1}\left(\frac{\rho_1}{\rho_2}\frac{h_1}{h_2} - \frac{\rho_2}{\rho_1}\frac{h_2}{h_1}\right) = 0, \tag{12}$$

$$\left[\frac{h_2}{h_1}(p_2+P_2) - (p_1+P_1)\right]\frac{\frac{h_2}{h_1}\rho_2}{\frac{h_2}{h_1}\rho_2 - \rho_1} = \gamma p_1 \mathcal{M}_1^2, \tag{13}$$

where $\mathcal{M}_1$ ($\equiv u_1/a_1$) is the Mach number of the upstream flow, a_1 ($\equiv \sqrt{\gamma p_1/\rho_1}$) being the sound speed in the upstream region. In addition to these Rankine–Hugoniot relations, we use the hydrostatic equilibrium relation:

$$\left(\frac{h_2}{h_1}\right)^2 = \frac{\rho_1}{\rho_2}\frac{p_2+P_2}{p_1+P_1}. \tag{14}$$

In the present radiative shock in disk accretion flows, there are four unknown variables (ρ_2, p_2, P_2, h_2). Inserting equations of state, $p = (\mathcal{R}/\mu)\rho T$ and $P = aT^4/3$, there remain three unknown variables (ρ_2, T_2, h_2) for three equations, and further eliminating ρ_2 and h_2, they are then combined into a single ninth-order polynomial equation on T_2 (e.g., Bouquet et al. 2000; Lowrie & Rauenzahn 2007). Here, in order to treat the problem semi-analytically, we consider the simplest two limits, the gas pressure and radiation pressure dominant cases.

2.3 Radiative precursor region

Using the solutions of the jump conditions as boundary conditions, the structure of the radiative precursor can be solved. For ideal gases and isotropic radiation fields, the energy conservation in equation (3) including the radiative flux is expressed as

$$h\frac{c}{\kappa\rho}\frac{dP}{dx} = h\frac{4acT^3}{3\kappa\rho}\frac{dT}{dx} = \left(\frac{1}{2}u^2 + \frac{\gamma}{\gamma-1}\frac{p}{\rho} + \frac{4P}{\rho}\right)h\rho u - \left(\frac{1}{2}u_1^2 + \frac{\gamma}{\gamma-1}\frac{p_1}{\rho_1} + \frac{4P_1}{\rho_1}\right)h_1\rho_1 u_1. \tag{15}$$

Eliminating u [$= h_1\rho_1 u_1/(h\rho)$], and again introducing the Mach number $\mathcal{M}_1$ ($= u_1/a_1$) in the upstream region, this equation can be rearranged as

$$\frac{h}{h_1}\frac{\rho_1}{\rho}\frac{\alpha_1}{\tau_1\beta_1}\frac{d}{d\tilde{x}}\frac{P}{P_1} = \frac{1}{2}\gamma\mathcal{M}_1^2\left[\left(\frac{\rho_1}{\rho}\right)^2\left(\frac{h_1}{h}\right)^2 - 1\right] + \frac{\gamma}{\gamma-1}\left(\frac{p}{p_1}\frac{\rho_1}{\rho} - 1\right) + 4\alpha_1\left(\frac{P}{P_1}\frac{\rho_1}{\rho} - 1\right), \tag{16}$$

where τ_1 ($\equiv \kappa\rho_1\ell_1$) is the typical optical depth, ℓ_1 the relevant scale length, β_1 ($\equiv u_1/c$) the normalized relative speed at the pre-shock region, and $\tilde{x}$ ($\equiv x/\ell_1$) the normalized coordinate.

Similarly, the momentum conservation in equation (2) is rearranged as

$$\frac{h}{h_1}p - p_1 + \frac{h}{h_1}P - P_1 = P_1\frac{\gamma}{\alpha_1}\mathcal{M}_1^2\left(1 - \frac{h_1}{h}\frac{\rho_1}{\rho}\right). \tag{17}$$

Parameters are τ_1, γ, α_1 ($\equiv P_1/p_1$), β_1 ($\equiv u_1/c$), and $\mathcal{M}_1^2$. From the physical viewpoints, we specify and separate these individual parameters. However, since τ_1 and β_1 are combined into a single parameter ($\tau_1\beta_1$), and furthermore, they are renormalized into the coordinate, the present radiative shock is a one-parameter family, such as $(\gamma/\alpha_1)\mathcal{M}_1^2$.

As was stated, in the following subsections we shall examine the two limiting cases.

3 Radiation–radiation shocks

In this section we shall examine *radiation–radiation* shocks, where the radiation pressure is dominant on both sides of the shock. In the usual one-dimensional radiative shocks, the radiation pressure dominated case is always a *continuous shock*.

3.1 Overall jump conditions

In the radiation pressure dominated case we drop the gas pressure terms, and the Rankine–Hugoniot relation of equation (12) and the hydrostatic relation of equation (14)

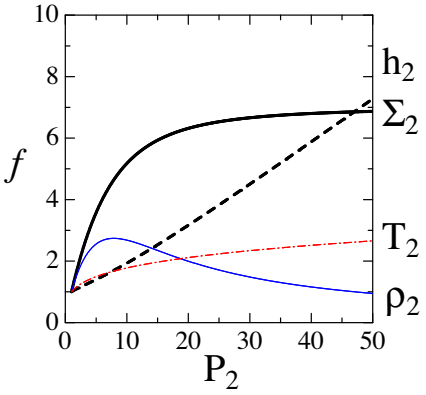

Fig. 2. Post-shock quantities as a function of $\tilde{P}_2$ in the radiation pressure dominated case. A thick solid curve represents $\tilde{\Sigma}_2$, a thin solid one $\tilde{\rho}_2$, a thick dashed one $\tilde{h}_2$, and a thin chain-dotted one $\tilde{T}_2$. (Color online)

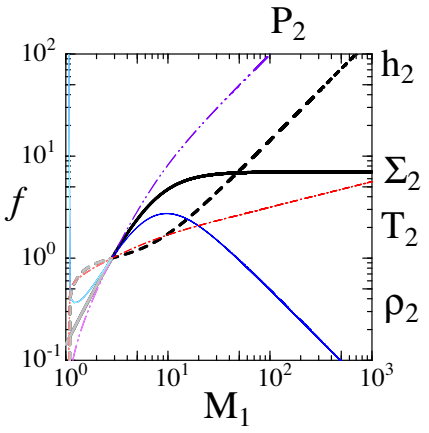

Fig. 3. Post-shock quantities as a function of $\mathcal{M}_1$ in the radiation pressure dominated case. A thick solid curve represents $\tilde{\Sigma}_2$, a thin solid one $\tilde{\rho}_2$, a thick dashed one $\tilde{h}_2$, a thin chain-dotted one $\tilde{T}_2$, and a thin two-dot chain one $\tilde{P}_2$. The parameters are $\gamma = 5/3$ and $\alpha_1 = 10$. (Color online)

become, respectively,

$$\frac{4P_2}{\rho_2} - \frac{4P_1}{\rho_1} + \frac{1}{2}\frac{\frac{h_2}{h_1}P_2 - P_1}{\frac{h_2}{h_1}\rho_2 - \rho_1}\left(\frac{\rho_1}{\rho_2}\frac{h_1}{h_2} - \frac{\rho_2}{\rho_1}\frac{h_2}{h_1}\right) = 0, \tag{18}$$

$$\frac{h_2^2}{h_1^2} = \frac{\rho_1}{\rho_2}\frac{P_2}{P_1}, \tag{19}$$

or, if the post-shock quantities are normalized by the pre-shock ones, these equations are re-expressed and arranged as:

$$7\frac{\tilde{P}_2}{\tilde{\rho}_2} - 7 + \frac{1}{\tilde{\rho}_2\tilde{h}_2} - \tilde{h}_2\tilde{P}_2 = 0, \tag{20}$$

$$\tilde{h}_2^2 = \frac{\tilde{P}_2}{\tilde{\rho}_2}, \tag{21}$$

where $\tilde{P}_2 = P_2/P_1$, $\tilde{\rho}_2 = \rho_2/\rho_1$, and $\tilde{h}_2 = h_2/h_1$.

Introducing the surface density Σ_2 ($\equiv h_2\rho_2$) instead of the density ρ_2 in the post-shock region, these equations are further rewritten as

$$7\frac{\tilde{P}_2}{\tilde{\Sigma}_2}\tilde{h}_2 - 7 + \frac{1}{\tilde{\Sigma}_2} - \tilde{h}_2\tilde{P}_2 = 0, \tag{22}$$

$$\tilde{\Sigma}_2\tilde{h}_2 = \tilde{P}_2, \tag{23}$$

and finally solved as

$$\tilde{\Sigma}_2 = \frac{1}{14}\left[1 - \tilde{P}_2^2 + \sqrt{(1-\tilde{P}_2^2)^2 + 196\tilde{P}_2^2}\right]. \tag{24}$$

Other post-shock quantities are given as, e.g., $\tilde{h}_2 = \tilde{P}_2/\tilde{\Sigma}_2$, $\tilde{\rho}_2 = \tilde{\Sigma}_2/\tilde{h}_2$, $\tilde{u}_2 = 1/\tilde{\Sigma}_2$, and $\tilde{T}_2 = \tilde{P}_2^{1/4}$.

In figure 2 several of these post-shock quantities are depicted as a function of $\tilde{P}_2$: a thick solid curve represents the surface density $\tilde{\Sigma}_2$, a thin solid one the density $\tilde{\rho}_2$, a thick dashed one the disk thickness $\tilde{h}_2$, and a thin chain-dotted one the radiation temperature $\tilde{T}_2$.

As is seen in figure 2, the gas density decreases for large $\tilde{P}_2$ due to the vertical expansion after the shock transition, although it increases for not so large $\tilde{P}_2$. Instead of the gas density, the surface density increases after the shock transition, and approaches 7 in the limit of large $\tilde{P}_2$.

On the other hand, another Rankine–Hugoniot relation, equation (13), becomes, in nondimensional form:

$$(\tilde{h}_2\tilde{P}_2 - 1)\frac{\tilde{h}_2\tilde{\rho}_2}{\tilde{h}_2\tilde{\rho}_2 - 1} = \frac{\gamma}{\alpha_1}\mathcal{M}_1^2, \tag{25}$$

where $\alpha_1 = P_1/p_1$.

Introducing the surface density Σ_2 ($\equiv h_2\rho_2$), this relation is further rewritten as

$$\frac{\tilde{P}_2^2 - \tilde{\Sigma}_2}{\tilde{\Sigma}_2 - 1} = \frac{\gamma}{\alpha_1}\mathcal{M}_1^2. \tag{26}$$

Now, using equations (22), (26), and (23), we can express the post-shock quantities as a function of the pre-shock Mach number as

$$\tilde{\Sigma}_2 = \frac{7(\gamma/\alpha_1)\mathcal{M}_1^2}{(\gamma/\alpha_1)\mathcal{M}_1^2 + 8}, \tag{27}$$

$$\tilde{P}_2^2 = \frac{[6(\gamma/\alpha_1)\mathcal{M}_1^2 - 1](\gamma/\alpha_1)\mathcal{M}_1^2}{(\gamma/\alpha_1)\mathcal{M}_1^2 + 8}; \tag{28}$$

here, $\tilde{h}_2 = \tilde{P}_2/\tilde{\Sigma}_2$, $\tilde{\rho}_2 = \tilde{\Sigma}_2/\tilde{h}_2$, and so on.

In figure 3, several of the post-shock quantities are depicted as a function of $\mathcal{M}_1$: a thick solid curve represents the surface density $\tilde{\Sigma}_2$, a thin solid one the density

$\tilde{\rho}_2$, a thick dashed one the disk thickness $\tilde{h}_2$, a thin chain-dotted one the radiation temperature $\tilde{T}_2$, and a thin two-dot chain one the radiation pressure $\tilde{P}_2$. The parameters are $\gamma = 5/3$ and $\alpha_1 = 10$. It should be stressed that the part for $\mathcal{M}_1 \leq 2.9$ is not realized, since $\tilde{P}_2$ and $\tilde{h}_2$ must be larger than unity. It should be further emphasized that a change of the parameter values is equivalent to a change of the Mach number, since they are combined into a single parameter $(\gamma/\alpha_1)\mathcal{M}_1^2$ in this radiation pressure dominated case; i.e., a single parameter family.

As is seen in figure 3, when the Mach number is not so large, the vertical expansion is not so effective, and the gas density slightly increases. When the Mach number becomes sufficiently large, due to the vertical expansion after the shock transition, the gas density decreases with Mach number as $\tilde{\rho}_2 \propto \mathcal{M}_1^{-1}$. Instead of the gas density, the surface density increases after the shock transition, and approaches 7 in the limit of large $\mathcal{M}_1$. The radiation pressure and thickness also increase after the shock transition, and both are proportional to the Mach number in the limit of large $\mathcal{M}_1$: $\tilde{P}_2, \tilde{h}_2 \propto \mathcal{M}_1$. In addition, $\tilde{T}_2 \propto \mathcal{M}_1^{1/4}$.

In addition, the disk relative thickness $\tilde{h}_2$ $(= h_2/h_1)$ of the post-shock region becomes quite large, up to the order of 10^2 in the present case. The validity of the disk scale height is discussed in section 5.

3.2 Radiative precursor structure

The structure equations for the radiative precursor in the radiation pressure dominated case can be expressed in terms of the variables $\tilde{P}$ $(\equiv P/P_1)$, $\tilde{\rho}$ $(\equiv \rho/\rho_1)$, and $\tilde{h}$ $(\equiv h/h_1)$ without T as

$$\frac{1}{\tau_1\beta_1}\frac{\tilde{h}}{\tilde{\rho}}\frac{d\tilde{P}}{d\tilde{x}} = \frac{1}{2}\frac{\gamma}{\alpha_1}\mathcal{M}_1^2\left(\frac{1}{\tilde{h}^2\tilde{\rho}^2} - 1\right) + 4\left(\frac{\tilde{P}}{\tilde{\rho}} - 1\right), \tag{29}$$

$$\tilde{h}\tilde{P} - 1 = \frac{\gamma}{\alpha_1}\mathcal{M}_1^2\left(1 - \frac{1}{\tilde{h}\tilde{\rho}}\right), \tag{30}$$

$$\tilde{h}^2 = \frac{\tilde{P}}{\tilde{\rho}}. \tag{31}$$

Again, introducing the surface density Σ $(\equiv h\rho)$, and eliminating h, we can obtain the following equations:

$$\frac{1}{\tau_1\beta_1}\frac{\tilde{P}^2}{\tilde{\Sigma}^3}\frac{d\tilde{P}}{d\tilde{x}} = \frac{1}{2}\frac{\gamma}{\alpha_1}\mathcal{M}_1^2\left(\frac{1}{\tilde{\Sigma}^2} - 1\right) + 4\left(\frac{\tilde{P}^2}{\tilde{\Sigma}^2} - 1\right), \tag{32}$$

$$\tilde{\Sigma} = \frac{\tilde{P}^2 + (\gamma/\alpha_1)\mathcal{M}_1^2}{1 + (\gamma/\alpha_1)\mathcal{M}_1^2}. \tag{33}$$

Using the overall jump relations of equations (27) and (28) as boundary conditions, we can easily solve equations (32) and (33) to obtain the radiative precursor structure.

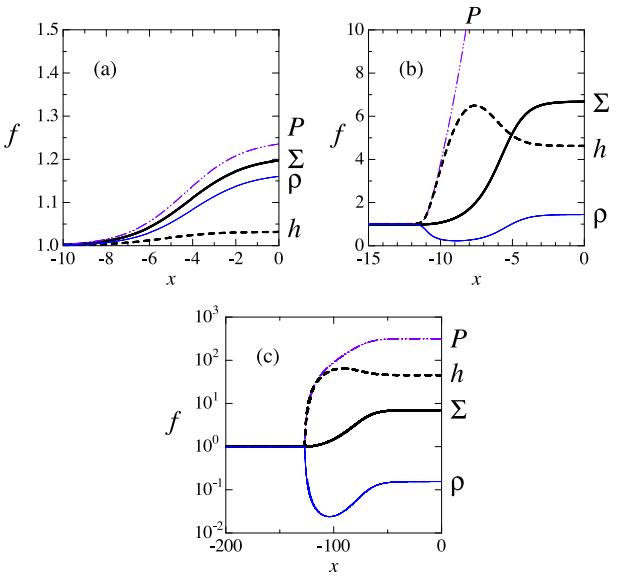

Fig. 4. Typical solutions for disk accretion radiative shocks in the radiation pressure dominated case as a function of the normalized coordinate. Thick solid curves represent the surface density $\tilde{\Sigma}$, thin solid ones $\tilde{\rho}$, thick dashed ones $\tilde{h}$, and thin two-dot chain ones $\tilde{P}$. The parameters are $\gamma = 5/3$, $\tau_1 = 100$, $\beta_1 = 0.01$, $\alpha_1 = 100$, and (a) $\mathcal{M}_1 = 10$, (b) $\mathcal{M}_1 = 10^2$, and (c) $\mathcal{M}_1 = 10^3$. The (surface) density distribution is continuous. (Color online)

Typical solutions for disk accretion radiative shocks in the radiation pressure dominated case are shown in figure 4 as a function of the normalized coordinate. Thick solid curves represent the surface density $\tilde{\Sigma}$, thin solid ones the gas density $\tilde{\rho}$, thick dashed ones the disk thickness $\tilde{h}$, and thin two-dot chain ones the radiation pressure $\tilde{P}$. The parameters are $\gamma = 5/3, \tau_1 = 100, \beta_1 = 0.01, \alpha_1 = 100$, and (a) $\mathcal{M}_1 = 10$, (b) $\mathcal{M}_1 = 10^2$, and (c) $\mathcal{M}_1 = 10^3$. As already mentioned, although we treat these individual parameters separately from the physical viewpoints, these solutions are a one-parameter family, e.g., $(\gamma/\alpha_1)\mathcal{M}_1^2$, since τ_1 and β_1 are renormalized into the coordinate. Hence, we fix all the parameters except for $\mathcal{M}_1$, and examine the dependence of solutions on the Mach number.

As is seen in figure 4, similar to the usual one-dimensional radiative shocks, the radiative energy from the hot post-shock region diffuses into the pre-shock region to make the radiative precursor. Furthermore, in contrast to hydrodynamical shocks, in radiation pressure dominated radiative shocks both the density and pressure distributions are continuous; i.e., so-called *continuous shocks*.

When the Mach number $\mathcal{M}_1$ in the pre-shock region is not so large and the shock is weak, as in figure 4a, the vertical expansion is small, and the gas density as well as the surface density increase, similar to the usual one-dimensional radiative shocks. When the Mach number $\mathcal{M}_1$ is large, as in figure 4b, due to the energy transport via radiative diffusion, the disk thickness quickly expands in the

radiative precursor region, and slightly decreases to settle down to the post-shock level. As a result, the gas density decreases at first, and then increases up to the post-shock level. However, the surface density monotonically increases to the post-shock level, similar to the gas density in the radiative precursor region of the simple one-dimensional radiative shocks under the radiation pressure dominated regime. When the Mach number $\mathcal{M}_1$ is sufficiently large, as in figure 4c, due to the vertical expansion the gas density in the post-shock region becomes smaller than that in the pre-shock region. Furthermore, the surface density compression approaches the maximum value of 7 in the radiation pressure dominated case.

4 Gas–gas shocks

In this section we shall examine *gas–gas* shocks, where the gas pressure is dominant on both sides of the shock. In the usual one-dimensional radiative shocks, the gas pressure dominated case is often an *isothermal shock* with discontinous density structure.

4.1 Overall jump conditions

In the gas pressure dominated case we drop the radiation pressure terms, and the Rankine–Hugoniot relation of equation (12) and the hydrostatic relation of equation (14) become, respectively,

$$\frac{\gamma+1}{\gamma-1}\frac{\tilde{p}_2}{\tilde{\rho}_2}-\frac{\gamma+1}{\gamma-1}+\frac{1}{\tilde{h}_2\tilde{\rho}_2}-\tilde{h}_2\tilde{p}_2=0, \tag{34}$$

$$\tilde{h}_2^2=\frac{\tilde{p}_2}{\tilde{\rho}_2}, \tag{35}$$

where $\tilde{p}_2 = p_2/p_1$, $\tilde{\rho}_2 = \rho_2/\rho_1$, and $\tilde{h}_2 = h_2/h_1$.

Introducing the surface density Σ_2 ($\equiv h_2\rho_2$) instead of the density ρ_2 in the post-shock region, these equations are further rewritten as

$$\frac{\gamma+1}{\gamma-1}\frac{\tilde{p}_2}{\tilde{\Sigma}_2}\tilde{h}_2-\frac{\gamma+1}{\gamma-1}+\frac{1}{\tilde{\Sigma}_2}-\tilde{h}_2\tilde{p}_2=0, \tag{36}$$

$$\tilde{\Sigma}_2\tilde{h}_2=\tilde{p}_2, \tag{37}$$

and finally solved as

$$\tilde{\Sigma}_2=\frac{\gamma-1}{2(\gamma+1)}\left[1-\tilde{p}_2^2+\sqrt{(1-\tilde{p}_2^2)^2+4\left(\frac{\gamma+1}{\gamma-1}\right)^2\tilde{p}_2^2}\right]. \tag{38}$$

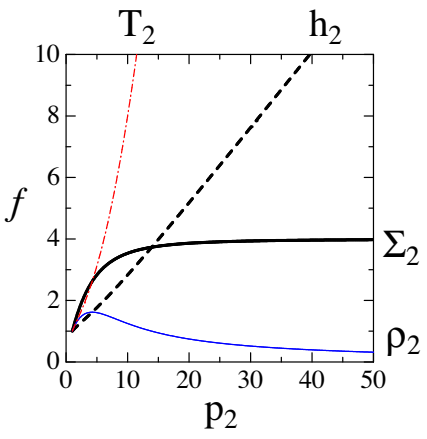

Fig. 5. Post-shock quantities as a function of $\tilde{p}_2$ in the gas pressure dominated case. A thick solid curve represents $\tilde{\Sigma}_2$, a thin solid one $\tilde{\rho}_2$, a thick dashed one $\tilde{h}_2$, and a thin chain-dotted one $\tilde{T}_2$. The parameter is $\gamma = 5/3$. (Color online)

Other post-shock quantities are given as, e.g., $\tilde{h}_2 = \tilde{p}_2/\tilde{\Sigma}_2$, $\tilde{\rho}_2 = \tilde{\Sigma}_2/\tilde{h}_2$, $\tilde{u}_2 = 1/\tilde{\Sigma}_2$, and $\tilde{T}_2 = \tilde{p}_2/\tilde{\rho}_2$.

In figure 5, several of these post-shock quantities are depicted as a function of $\tilde{p}_2$: a thick solid curve represents the surface density $\tilde{\Sigma}_2$, a thin solid one the density $\tilde{\rho}_2$, a thick dashed one the disk thickness $\tilde{h}_2$, and a thin chain-dotted one the radiation temperature $\tilde{T}_2$. The parameter is $\gamma = 5/3$.

As is seen in figure 5, similar to the radiation dominated case, the gas density decreases for large $\tilde{p}_2$ due to the vertical expansion after the shock transition, although it increases for not so large $\tilde{p}_2$. Instead of the gas density, the surface density increases after the shock transition, and approaches 4 in the limit of large $\tilde{p}_2$ in the gas pressure dominated case ($\gamma = 5/3$). In this case, furthermore, the post-shock temperature $\tilde{T}_2$ steeply increases compared with that of the radiation pressure dominated case in figure 2. In addition, if the gas is relativistic and $\gamma = 4/3$, except for the temperature, the behavior of these quantities is same as those in the radiation pressure dominated case.

On the other hand, another Rankine–Hugoniot relation, equation (13), becomes, in nondimensional form:

$$(\tilde{h}_2\tilde{p}_2-1)\frac{\tilde{h}_2\tilde{\rho}_2}{\tilde{h}_2\tilde{\rho}_2-1}=\gamma\mathcal{M}_1^2. \tag{39}$$

Introducing the surface density Σ_2 ($\equiv h_2\rho_2$), this relation is further rewritten as

$$\frac{\tilde{p}_2^2-\tilde{\Sigma}_2}{\tilde{\Sigma}_2-1}=\gamma\mathcal{M}_1^2. \tag{40}$$

Now, using equations (36), (40), and (37), we can express the post-shock quantities as a function of the

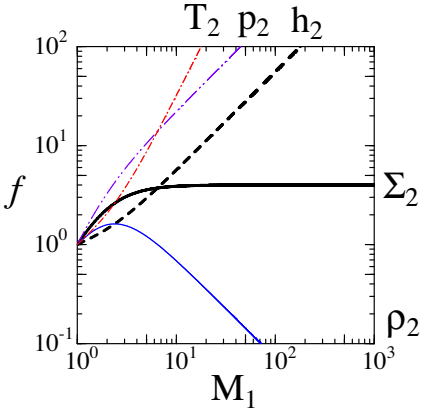

Fig. 6. Post-shock quantities as a function of $\mathcal{M}_1$ in the gas pressure dominated case. A thick solid curve represents $\tilde{\Sigma}_2$, a thin solid one $\tilde{\rho}_2$, a thick dashed one $\tilde{h}_2$, a thin chain-dotted one $\tilde{T}_2$, and a thin two-dot chain one $\tilde{p}_2$. The parameter is $\gamma = 5/3$. (Color online)

pre-shock Mach number as

$$\tilde{\Sigma}_2 = \frac{(\gamma+1)\mathcal{M}_1^2}{(\gamma-1)\mathcal{M}_1^2+2}, \tag{41}$$

$$\tilde{p}_2^2 = \frac{(2\gamma\mathcal{M}_1^2+1-\gamma)\mathcal{M}_1^2}{(\gamma-1)\mathcal{M}_1^2+2}, \tag{42}$$

where $\tilde{h}_2 = \tilde{p}_2/\tilde{\Sigma}_2$, $\tilde{\rho}_2 = \tilde{\Sigma}_2/\tilde{h}_2$, $\tilde{T}_2 = \tilde{p}_2/\tilde{\rho}_2$, and so on. It should be noted that the surface density expression of equation (41) is quite similar to the gas density expression in the usual hydrodynamical shock, although other expressions are not.

In figure 6, several of the post-shock quantities are depicted as a function of $\mathcal{M}_1$: a thick solid curve represents the surface density $\tilde{\Sigma}_2$, a thin solid one the density $\tilde{\rho}_2$, a thick dashed one the disk thickness $\tilde{h}_2$, a thin chain-dotted one the radiation temperature $\tilde{T}_2$, and a thin two-dot chain one the radiation pressure $\tilde{p}_2$. The parameter is $\gamma = 5/3$.

As is seen in figure 6, similar to the radiation pressure dominated case, when the Mach number is not so large the vertical expansion is not so effective, and the gas density slightly increases. When the Mach number becomes sufficiently large, due to the vertical expansion after the shock transition, the gas density decreases with Mach number as $\tilde{\rho}_2 \propto \mathcal{M}_1^{-1}$. Instead of the gas density, the surface density increases after the shock transition, and approaches 4 in the limit of large $\mathcal{M}_1$. The gas pressure and thickness also increase after the shock transition, and both are proportional to the Mach number in the limit of large $\mathcal{M}_1$:$\tilde{p}_2$, $\tilde{h}_2 \propto \mathcal{M}_1$. In contrast to the radiation pressure dominated case, the gas temperature steeply increases, and it depends on the Mach number as $\tilde{T}_2 \propto \mathcal{M}_1^2$ in the limit of large $\mathcal{M}_1$.

Similar to the radiation–radiation shock, the disk relative thickness $\tilde{h}_2$ of the post-shock region becomes quite large, up to the order of 10^2, in the present case. This point is also discussed in section 5.

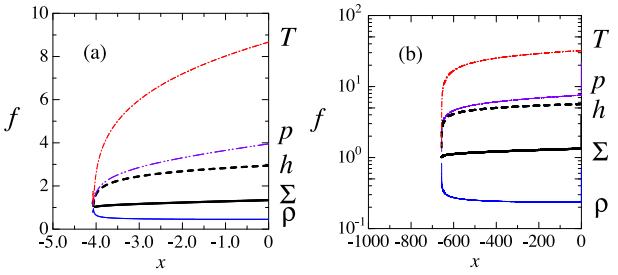

Fig. 7. Typical solutions for disk accretion radiative shocks in the gas pressure dominated case as a function of the normalized coordinate. Thick solid curves represent the surface density $\tilde{\Sigma}$, thin solid ones ρ, thick dashed ones $\tilde{h}$, thin chain-dotted ones $\tilde{T}$, and thin two-dot chain ones $\tilde{p}$. The parameters are $\gamma = 5/3$, $\tau_1 = 100$, $\beta_1 = 0.0001$, $\alpha_1 = 0.00001$, and (a) $\mathcal{M}_1 = 5$, (b) $\mathcal{M}_1 = 10$. The (surface) density distribution is discontinuous, while the temperature one is continuous. (Color online)

4.2 Radiative precursor structure

The structure equations for the radiative precursor in the gas pressure dominated case can be expressed in terms of variables $\tilde{T}$ ($\equiv T/T_1$), $\tilde{\rho}$ ($\equiv \rho/\rho_1$), and $\tilde{h}$ ($\equiv h/h_1$) as

$$\frac{4\alpha_1}{\tau_1\beta_1}\frac{\tilde{h}\tilde{T}^3}{\tilde{\rho}}\frac{d\tilde{T}}{d\tilde{x}} = \frac{1}{2}\gamma\mathcal{M}_1^2\left(\frac{1}{\tilde{h}^2\tilde{\rho}^2}-1\right)+\frac{\gamma}{\gamma-1}\left(\tilde{T}-1\right), \tag{43}$$

$$\tilde{h}\tilde{\rho}\tilde{T}-1 = \gamma\mathcal{M}_1^2\left(1-\frac{1}{\tilde{h}\tilde{\rho}}\right), \tag{44}$$

$$\tilde{h}^2 = \frac{\tilde{p}}{\tilde{\rho}} = \tilde{T}, \tag{45}$$

where $\tau_1 = \kappa\rho_1\ell_1$, $\beta_1 = u_1/c$, and $\alpha_1 = P_1/p_1$.

Again, introducing the surface density Σ ($\equiv h\rho$) and eliminating h, we can obtain the following equations:

$$\frac{4\alpha_1}{\tau_1\beta_1}\frac{\tilde{T}^4}{\tilde{\Sigma}}\frac{d\tilde{T}}{d\tilde{x}} = \frac{1}{2}\gamma\mathcal{M}_1^2\left(\frac{1}{\tilde{\Sigma}^2}-1\right)+\frac{\gamma}{\gamma-1}\left(\tilde{T}-1\right), \tag{46}$$

$$\tilde{\Sigma} = \frac{1}{2\tilde{T}}\left[1+\gamma\mathcal{M}_1^2-\sqrt{(1+\gamma\mathcal{M}_1^2)^2-4\gamma\mathcal{M}_1^2\tilde{T}}\right]. \tag{47}$$

Using the overall jump relations as boundary conditions, we can solve equations (46) and (47) to obtain the radiative precursor structure.

Typical solutions for disk accretion radiative shocks in the gas pressure dominated case are shown in figure 7 as a function of the normalized coordinate. Thick solid curves represent the surface density $\tilde{\Sigma}$, thin solid ones the gas density $\tilde{\rho}$, thick dashed ones the disk thickness $\tilde{h}$, thin chain-dotted ones the gas temperature $\tilde{T}$, and thin two-dot chain ones the radiation pressure $\tilde{p}$. The parameters are $\gamma = 5/3$,

$\tau_1 = 100$, $\beta_1 = 0.0001$, $\alpha_1 = 0.00001$, and (a) $\mathcal{M}_1 = 5$, (b) $\mathcal{M}_1 = 10$. As already mentioned, although we treat these individual parameters separately from the physical viewpoints, these solutions are a one-parameter family, e.g., $\gamma\mathcal{M}_1^2$, since τ_1, β_1, and α_1 are renormalized into the coordinate. Hence, we fix all the parameters except for $\mathcal{M}_1$, and examine the dependence of solutions on the Mach number.

As is seen in figure 7, similar to the usual one-dimensional radiative shocks, the radiative energy from the hot post-shock region diffuses into the pre-shock region to make the radiative precursor. Furthermore, in contrast to the radiation pressure dominated case, the (surface) density distribution is discontinuous, although the temperature distribution is continuous; i.e., the so-called *isothermal shocks*. Namely, in contrast to the radiation pressure dominated case, in this gas pressure dominated case the surface density of equation (47) in the radiative precursor just before the shock front is usually smaller than the surface density of equation (41) in the post-shock region.

Furthermore, in the gas pressure dominated case, due to the quick heating and quick expansion in the radiative precursor region, the gas density decreases while the surface density increases.

5 Discussion

In this section we shall discuss the validity of several assumptions in the present study.

5.1 Disk scale height

As was stated, due to the shock heating, in the post-shock region the disk relative thickness $\tilde{h}_2$ ($= h_2/h_1$) becomes quite large, up to the order of 10^2 in the present parameter range. We then briefly check the post-shock scale height.

The scale height h_2/r to radius r in the post-shock region is expressed as

$$\frac{h_2}{r} = \tilde{h}_2 \frac{h_1}{r}. \tag{48}$$

Hence, the post-shock scale height h_2/r would not exceed unity, as long as the condition for the pre-shock scale height of

$$\frac{h_1}{r} < \tilde{h}_2^{-1} \tag{49}$$

is satisfied. For $\tilde{h} \sim 10^2$, this condition means $h_1/r < 0.01$, which is easily satisfied for disk accretion flow of cold gas.

We further estimate this condition using the solutions of the standard accretion disk (e.g., Kato et al. 2008), although the present situation assumes accretion flow with low angular momentum. For example, in the radiation pressure dominated inner region of the standard accretion disk, the scale height is roughly $H/r \sim 0.2\dot{m}\hat{r}^{-1}$, where $\dot{m}$ is the mass accretion rate normalized by the critical rate, and $\hat{r} = r/r_{\rm S}$, $r_{\rm S}$ being the Schwarzschild radius of the central object. Thus, for $\dot{m} \lesssim 0.1$, the above condition is satisfied.

In the gas pressure dominated middle region of the standard accretion disk, the scale height is roughly $H/r \sim 0.01\alpha^{-1/10}m^{-1/10}\dot{m}^{1/5}\hat{r}^{-1/20}$, where α is the alpha parameter, and $m = M/M_\odot$. Thus, the above condition is easily satisfied when $\tilde{h}_2 < 10^2$.

If, however, the mass accretion rate is large, or the shock becomes much stronger beyond the present range, the post-shock relative scale height would exceed unity. In such a case, the shocked gas would no longer be gravitationally bound, and would puff up to blow off from the shocked disk (see, e.g., Kim et al. 2019 for hydrodynamical shocks).

5.2 Hydrostatic balance

We have assumed hydrostatic balance in the vertical direction in the precursor region as well as on both sides of the shocks. If the timescale that the flow goes across the transition layers δr with velocity u, $\delta r/u$, is shorter than the sound crossing time in the vertical direction h/a (a being the sound speed), this assumption would be violated.

If we evaluate these quantities by those after the shock, and replace δr by r, for the hydrostatic balance to be quickly established we need

$$\mathcal{M}_2 \frac{h_2}{r} < 1, \tag{50}$$

where $\mathcal{M}_2 = u_2/a_2 < 1$. Hence, as long as the relative thickness h_2/r after the shock front is less than unity, the hydrostatic balance would hold in the present case.

5.3 Equilibrium diffusion approximation

In this paper we adopt the equilibrium diffusion approximation in the optically thick regime ($1T$ limit). Since the gas temperature rapidly increases at the shock, the radiation temperature cannot immediately equilibrate the gas temperature at the post-shock region in some situations (nonequilibrium diffusion regime; $2T$ limit).

In order to equilibrate radiation and matter, the energy exchange timescale between radiation and matter should be shorter than the dynamical timescale. Of these, the dynamical timescale $t_{\rm dyn}$ is roughly

$$t_{\rm dyn} \sim \frac{\ell}{u_1}, \tag{51}$$

where ℓ is the typical scale length, and u_1 the flow speed before the shock front, which is larger than u_2.

The variation timescale of the radiation energy density E can be estimated using the zeroth moment equation of the radiation field:

$$\frac{\partial E}{\partial t} + \nabla \cdot \boldsymbol{F} = \kappa\rho(4\pi B - cE), \tag{52}$$

where LTE is assumed, and B is the blackbody intensity. Using the gas temperature $T_{\rm gas}$ and radiation temperature $T_{\rm rad}$, $B = \sigma_{\rm SB}T_{\rm gas}^4$ and $E = aT_{\rm rad}^4$ ($ac/4 = \sigma_{\rm SB}$). Hence, the variation timescale $t_{\rm rad}$ of the radiation energy density roughly becomes

$$t_{\rm rad} \sim \frac{E}{\kappa\rho 4\pi B} \sim \frac{1}{\kappa\rho c\pi}\frac{T_{\rm rad}^4}{T_{\rm gas}^4} \sim \frac{1}{\tau}\frac{\ell}{c}\frac{T_{\rm rad}^4}{T_{\rm gas}^4}, \tag{53}$$

where $\tau = \kappa\rho\ell$ is the typical optical depth. Thus, for $t_{\rm rad} < t_{\rm dyn}$, the condition

$$\frac{u_1}{c}\frac{1}{\tau} < \frac{T_{\rm gas}^4}{T_{\rm rad}^4} \tag{54}$$

must be satisfied. Since the gas temperature is larger than the radiation temperature after the shock front, this condition is usually satisfied for nonrelativistic, optically thick flows.

On the other hand, the variation timescale of the gas internal energy U [$(\gamma - 1)U = p/\rho$ for ideal gas] can be estimated using the energy equation for matter:

$$\frac{1}{\gamma - 1}\left(\frac{dp}{dt} - \gamma\frac{p}{\rho}\frac{d\rho}{dt}\right) = -\rho(4\pi\kappa B - c\kappa E), \tag{55}$$

where we again assume LTE. Hence, the variation timescale $t_{\rm gas}$ of the gas internal energy is roughly expressed as

$$t_{\rm gas} \sim \frac{1}{\gamma - 1}\frac{p}{\rho c\kappa E} \sim \frac{1}{\tau}\frac{\ell}{c}\frac{p}{P}, \tag{56}$$

where we adopt the Eddington approximation: $E = 3P$. Thus, the condition for $t_{\rm gas} < t_{\rm dyn}$ becomes

$$\frac{u_1}{c}\frac{1}{\tau} < \frac{P}{p}. \tag{57}$$

For a radiation pressure dominated shock this condition is usually satisfied. Even for the gas pressure dominated case this condition can be satisfied if the flow is sufficiently slow and/or sufficiently optically thick. Otherwise, the present $1T$ approximation would be violated and we should treat the radiative shock under the nonequilibrium diffusion regime.

6 Concluding remarks

In this paper we first examined radiative shocks in disk accretion flows under the condition of hydrostatic balance in the vertical direction, and using the equilibrium diffusion and Eddington approximations in the optically thick regime. We derived the overall jump conditions for such disk accretion shocks, and solved the structure of the radiative precursor region for both the gas and radiation pressure dominated cases. In contrast to the usual one-dimensional radiative shocks, where the gas density of the post-shock region increases due to the shock compression, if the shock is sufficiently strong, the gas density in the post-shock region often decreases due to the vertical expansion behind the shock front. However, the surface density behaves like the gas density in usual shocks, and increases up to 7 in the radiation pressure dominated case. Hence, the vertical optical depth in the post-shock region rises, in spite of the reduction of the gas density. In addition, similar to the usual radiative shocks, a radiative precursor appears in the pre-shock region before the shock front, due to the radiative diffusion effect.

The solutions are quite fundamental in disk accretion shock problems, and should be developed in various aspects. We shall enumerate some of them:

Diffusion approximation: In this paper we adopt the equilibrium diffusion approximation in the optically thick regime, and consider the gas pressure and radiation pressure dominant cases, in order to treat the problem semi-analytically. If we consider both the gas and radiation pressures simultaneously, the resultant equations may be combined into a single ninth-order polynomial equation on T_2, similar to the one-dimensional radiative shock (e.g., Bouquet et al. 2000; Lowrie & Rauenzahn 2007). Furthermore, in the nonequilibrium diffusion regime ($2T$ limit), at the post-shock region some type of relaxation zone appears, as well as the gas temperature peak called the *Zel'dovich spike*. In addition, we adopt the Eddington approximation to close the radiative moment equations. In order to treat the radiative shock more accurately, we should solve the radiative transfer equation numerically, although such work is rare at the moment (e.g., Tolstov et al. 2015).

Optical depth: We assume that the disk material is optically thick in both the pre-shock and post-shock regions; that is, we examine a *thick–thick* shock (cf. Drake 2005). If the gas in the pre-shock region is optically thin, as in advection dominated accretion flows (ADAFs), then *thin–thick* and *thin–thin* shocks may appear, although the thick–thin shock is difficult to realize in nature.

Radiative cooling: The radiative cooling from the disk surface in the optically thick case, and from the entire

shocked flow in the optically thin case, is also important, especially in the post-shock region.

Spectral properties: Chakrabarti and Titarchuk (1995) studied the spectral properties of an optically thick disk with a hot inner post-shock region with optical depth on the order of unity. However, as was already mentioned, the surface density, and therefore the optical depth, in the post-shock region must further increase compared with the outer pre-shock disk in both nonradiative and radiative shocks under hydrostatic equilibrium. Hence, the spectral properties of radiative shocks in disk accretion should also be re-examined.

Radiative winds: In the present optically thick shock, the surface density increases after shock transition, and therefore the optical depth also becomes large. Hence, in the post-shock region the optically thick wind would be launched by the strong radiation pressure (see, e.g., Chattopadhyay & Chakrabarti 2002 for the hydrodynamical shock case). If the optically thick wind blows off the post-shock region, the naked surface is obscured and the spectral properties should be drastically changed.

Transonic flows: As in hydrodynamical shocks, radiative shocks can be incorporated into transonic accretion flows onto the central gravitating object (e.g., Fukue 1987). In contrast to hydrodynamical shocks, which can be treated as a discontinuity with no width, radiative shocks generally have a radiative precursor with a finite width. Hence, radiative shocks in transonic accretion flows onto the central object should be examined carefully, since, e.g., the gravitational field would change during shock transition.

Magnetohydrodynamic radiative shocks: Toroidal magnetic fields are easily incorporated into a viscous accretion flow around a central object. For example, Akizuki and Fukue (2006) found self-similar solutions for ADAFs with toroidal magnetic fields. Radiative shocks in magnetized disk accretion are also important problems.

Propagating radiative shocks: In the present study, we bear in mind the standing radiative shocks in the disk accretion flows. Due to the strong explosion at the center of accretion disks, e.g., novae and X-ray bursts, shock waves are caused and propagate in the disk (e.g., Fukue 1982). With the help of the Galilean transformation, standing radiative shocks are easily applied to the propagating radiative shocks.

Supercritical accretion flows: If the mass accretion rate is sufficiently large, the accretion disk is no longer geometrically thin but puffs up to make a geometrically thick supercritical accretion flow (e.g., Kato et al. 1998, 2008). In general, radiative shocks in such two-dimensional flows are treated by numerical simulations. However, in self-similar supercritical accretion flows (e.g., Watarai & Fukue 1999; Fukue 2004 and references therein), the radiative shocks could be examined semi-analytically.

Numerical simulations: Okuda et al. (2004) performed one- and two-dimensional numerical simulations of radiative shocks in rotating accretion flows around black holes. In their results, the radiative precursor and maybe the Zel'dovich spike are seen, but they did not mention these properties from the viewpoints of radiative shocks. Recently, Marleau et al. (2017) carried out one-dimensional and one-temperature (1T) radiation-hydrodynamical simulations of the planetary accretion shock at the surface of a planet. They found that the shock is isothermal and supercritical for a range of the relevant parameters. The present study on radiative shocks in disk accretion may be quite useful to analyze and understand radiative shocks in numerical simulations.

Relativity: Since radiative shocks in accretion flows may be associated with nonrelativistic disk accretion, such as protoplanetary disks, we first examined nonrelativistic radiative shocks. In the case of relativistic disk accretion onto a compact object, however, both flow speed and temperature become relativistic, and we should consider relativistic radiative shocks (e.g., Taub 1948; Thorne 1973; Gao & Law 2012; Fukue 2019a), as in the relativistic hydrodynamical shock in disk accretion by Fukue (1987). Hence, special relativistic treatment with the relativistic equation of state should first be necessary (Fukue 2019b). When the gas temperature changes from the nonrelativistic one before the shock to the relativistic one after the shock, the rigorous equation of state should be applied. When the flow speed is relativistic the radiation field becomes anisotropic, and the relativistic radiative transfer should be solved (cf. Tolstov et al. 2015 for the one-dimensional special relativistic case). Finally, when the radiative shock is not discontinuous, but has a radiative precursor and thermalization region with some width, the general relativistic gravitational effect is also important.

Stability: Stability of the shock front is also an important problem. It is well known that accretion shock is unstable to non-axisymmetric perturbations (e.g., Nagakura & Yamada 2008). In addition to non-axisymmetric perturbations, the shock structure would be unstable in the multi-dimensional model (e.g., Kim et al. 2019). The stability and oscillations of the radiative shocks in disk accretion should be examined in the future.

Anyway, as was stated in the introduction, the present work is only a starting point for radiative shocks in disk accretion and more general flows around the central object.

Many unresolved issues remain to be reexamined and developed in the future.

Acknowledgments

The author would like to thank an anonymous referee for useful comments to clarify the validity of several assumptions. This work has been supported in part by a Grant-in-Aid for Scientific Research (18K03701) of the Ministry of Education, Culture, Sports, Science and Technology.

References

Akizuki, C., & Fukue, J. 2006, PASJ, 58, 469
Bouquet, S., Teyssier, R., & Chieze, J. P. 2000, ApJS, 127, 245
Chakrabarti, S. A. 1989, ApJ, 347, 365
Chakrabarti, S. A. 1996, ApJ, 464, 664
Chakrabarti, S. A., & Das, S. D. 2004, MNRAS, 349, 649
Chakrabarti, S. A., & Titarchuk, L. G. 1995, ApJ, 455, 623
Chattopadhyay, I., & Chakrabarti, S. K. 2002, MNRAS, 333, 454
Das, T. K. 2002, ApJ, 577, 880
Drake, R. P. 2005, Ap&SS, 298, 49
Drake, R. P. 2007, Phys. Plasma, 14, 043301
Ferguson, J. M., Morel, J. E., & Lowrie, R. B. 2017, arXiv:1702.07300v1
Fukue, J. 1982, PASJ, 34, 483
Fukue, J. 1987, PASJ, 39, 309
Fukue, J. 2004, PASJ, 56, 569
Fukue, J. 2019a, MNRAS, in press
Fukue, J. 2019b, MNRAS, in press
Gao, Y., & Law, C. K. 2012, ApJ, 760, 122
Kato, S., Fukue, J., & Mineshige, S. 1998, Black-Hole Accretion Disks (Kyoto: Kyoto University Press)
Kato, S., Fukue, J., & Mineshige, S. 2008, Black-Hole Accretion Disks – Toward a New Paradigm (Kyoto: Kyoto University Press)
Kim, J., Garain, S. K., Chakrabarti, S. K., & Balsara, D. S. 2019, MNRAS, 482, 3636
Lacey, C. G. 1988, ApJ, 326, 769
Lowrie, R. B., & Edwards, J. D. 2008, Shock Waves, 18, 129
Lowrie, R. B., Morel, J. E., & Hittinger, J. A. 1999, ApJ, 521, 432
Lowrie, R. B., & Rauenzahn, R. M. 2007, Shock Waves, 16, 445
Lu, J.-F., & Yuan, F. 1997, PASJ, 49, 525
Marleau, G.-D., Klahr, H., Kuiper, R., & Mordasini, C. 2017, ApJ, 836, 221
Mihalas, D., & Mihalas, B. W. 1984, Foundations of Radiation Hydrodynamics (Oxford: Oxford University Press)
Nagakura, H., & Yamada, S. 2008, ApJ, 689, 391
Okuda, T., Teresi, V., Toscano, E., & Molteni, D. 2004, PASJ, 56, 547
Raizer, Y. P. 1957, Sov. Phys. JETP, 5, 1242
Suková, P., Charzyński, S., & Janiuk, A. 2017, MNRAS, 472, 4327
Taub, A. H. 1948, Phys. Rev., 74, 328
Thorne, K. S. 1973, ApJ, 179, 897
Tolstov, A., Blinnikov, S., Nagataki, S., & Nomoto, K. 2015, ApJ, 811, 47
Watarai, K., & Fukue, J. 1999, PASJ, 51, 725
Weaver, T. A. 1976, ApJS, 32, 233
Zel'dovich, Y. B. 1957, Sov. Phys. JETP, 5, 919
Zel'dovich, Y. B., & Raizer, Y. P. 1966, Physics of Shock Waves and High-Temperature Hydrodynamic Phenomena, Vol. 1 (New York: Academic Press)
Zel'dovich, Y. B., & Raizer, Y. P. 2002, Physics of Shock Waves and High-Temperature Hydrodynamic Phenomena (New York: Dover)